Non-intrusive in-line rheometry using ultrasonic velocity profiling

Yuji Tasaka,*,† Taiki Yoshida,‡ and Yuichi Murai†

†*Faculty of Engineering, Hokkaido University, Sapporo 060-8628, Japan*

‡*National Metrology Institute of Japan, National Institute of Advanced Industrial Science and Technology, Tsukuba 305-8560, Japan*

E-mail: tasaka@eng.hokudai.ac.jp

Abstract

We present a new approach to realize non-intrusive in-line rheometry without measuring the pressure difference along the pipe, which is required in conventional methods that insert pressure probes in the pipe. The rheometry utilizes unsteadiness of target pipe flows reflected by spatio-temporal velocity information. The quasi-instantaneous rheological properties were estiamted by inverse analysis of the equation of motion, which governs unsteady one-directional pipe flows, in the frequency domain. To evaluate applicability of the present in-line rheometry as 'viscometry', numerical experiment was performed using solution of pulsatile pipe flows with different viscosities and frequencies. The limitations of the viscosity measurement range considering the thickness of the viscous layer formed on the pipe wall are discussed. We demonstrated the utility of our method on a laboratory pipe loop facility with a viscous silicone oil as the test fluid. Finally, we quantified the time variation of the viscosity due to transient temperature variation of the fluid.

Introduction

In-line monitoring of rheological properties, such as viscosity and viscoelasticity, is important for ensuring the high quality of food, chemical and material products, optimizing processes, and for safe processing of the products. Conventional pressure difference measurements along a pipe quantify the frictional force acting on the pipe wall. This relies on assumptions of the type of fluid (e.g. Newtonian, pseudo-plastic, Bingham plastic). Furthermore, slip of the fluid flow on the wall causes considerable errors in the estimations of rheological properties. Differences in fluid type and existence of the slip appear in the velocity profile in a pipe, and supplemental information of velocity profile is thus introduced to improve the accuracy of estimation.

Wunderlich & Brunn[1] used an ultrasonic velocity profiler (UVP)[2] that can measure the instantaneous velocity profile in the direction of ultrasound propagation in clear and opaque liquids. They assumed fully developed, steady laminar flows with wall slip and shear-dependent viscosity, and derived a relation between the velocity profile and wall shear stress calculated from the pressure difference. The shear-dependent viscosity was estimated via function fitting on the velocity data, and influence of the fitting functions was evaluated. Ouriev & Windhab[3] proposed a similar method, which they termed UVP-PD (pressure difference), to estimate shear-rate-dependent viscosity. Different rheology models were chosen depending on the test fluids and the rheological properties were determined also by function fitting on the velocity profiles measured by UVP. The UVP-PD method has been used for various fluids, such as suspensions,[4,5] tomato sauce,[6] cocoa butter,[7,8] viscoelastic surfactant solution,[9] and cement grouts.[10,11] The method has been advanced by monitoring of the speed of sound through the test fluid to ensure highly accurate measurement of the velocity profile,[12] and using an optimized transducer to reduce the lack of the velocity profile data near the wall.[13] The latter approach achieves clamp-on technology, which allows non-intrusive measurement of the velocity profiles for industrial applications. Model-free estimation of the shear profiles in a pipe flow of a pseudo-plastic fluid was examined using spline inter-

polation of the velocity data.[14] The authors discussed the influence of the large velocity gradient near the pipe wall (due to the shear thinning) on the velocity-profile measurement. A problem using such in-line measurement systems is that it is necessary to measure the pressure difference, which requires the use of intrusive probes in the pipes. This is potential sanitary problem. Furthermore, the assumption of steady flow limits the range of applicable targets and properties that can be evaluated; for example, viscoelasticity, which is a typical rheological property, cannot be evaluated using UVP-PD method.

UVP-assisted method (such as UVP-PD) for estimating rheological properties have been used for cylindrical systems, which are conventionally used for torque-type rheometers. For example, Derakhshandeh *et al.*[15] used this approach for fiber suspensions to quantify shear-thinning viscosity and yield stress. Manneville *et al.*[16] also used a cylindrical system with ultrasonic speckle velocimetry with high-speed ultrasonic imaging instead of UVP, and evaluated the rheological properties of surfactant solutions in a lyotropic lamellar phase that exhibited slip on the wall and shear banding. Gallot *et al.*[17] advanced the technique and applied it to a wormlike micellar solution that also exhibited shear banding.

Our research group recently established a conceptually different UVP-assisted method – ultrasonic spinning rheometry (USR)[18–21] This method uses time variations of the velocity profiles measured by UVP in a cylindrical vessel filled with the test fluid driven by oscillatory rotations of the vessel. The velocity data are substituted into the equation of motion describing unsteady, one-directional flow in the cylinder, and a rheological model as a constitutive equation. Rheological properties of the test fluids are estimated by solving the optimization problem on the equations without axial torque information. This is different to other UVP-assisted methods. To avoid augmentation of the measurement error in the velocity data by numerical differentiation to solve the equation of motion numerically, data processing is performed in the frequency domain with the component corresponding to the oscillation frequency of the test cylinder.

Depending on the specific rheological model used, USR can evaluate the effective viscosity,

shear-rate-dependent viscosity, and effective viscoelasticity. USR can be applied to wide range of fluids, such as polymer solutions,[21,22] bubble suspensions,[18,20] particle suspensions in non-Newtonian fluids,[22] clay dispersions,[21,23] and pectin gels.[23,24] We evaluated the efficacy and measurable range of USR for different materials by comparison with a standard torque-type rheometer.[21] Some of the advantages of USR include its applicability for multiphase and heterogeneous fluids, and for evaluating the transient behavior of the fluids like thixotropy and chemical reactions.

The present study establishes non-intrusive in-line rheometry by utilizing the concept of USR to eliminate the need to measure the pressure difference. We achieved this by optimization analysis of the equation of motion and rheological models substituted by spatio-temporal velocity data measured by UVP in the frequency domain. The concept, theoretical details, and limitations of this in-line rheometry are detailed in the following sections. We evaluated the applicability of the present method as in-line 'viscometry' numerically using velocity data generated from an analytical solution of pulsatile pipe flows with different viscosities and frequencies of velocity fluctuations. Finally, the method was demonstrated on pulsatile pipe flows of a silicone oil with transient temperature variations in a laboratory pipe loop facility.

Theory

Basic concept

Unsteady laminar pipe flows with an axisymmetric velocity profile can be described by the following equation of motion:

$$\rho \frac{\partial u}{\partial t} = \alpha(t) + \frac{\partial \tau}{\partial r} + \frac{\tau}{r}, \tag{1}$$

where ρ and $\alpha(t) = -\partial p/\partial x$ denote the density and unsteady pressure gradient in the flow direction x. The relationship between the shear stress, τ, and the shear rate, $\dot{\gamma}$, is expressed

by the rheological model as a constitutive equation,

$$\tau = h(\dot{\gamma}; \Pi_1, \Pi_2, \Pi_3, \cdots), \ \dot{\gamma} = \frac{\partial u}{\partial r} \tag{2}$$

with constants, $\Pi_1, \Pi_2, \Pi_3, \cdots$, which represent rheological properties, e.g. the power index and the viscosity coefficient in the power law model describing shear-rate-dependent viscosity. Assuming that the velocity profile $u(r,t)$ is given by the UVP measurements, the equation system of Eq. 1 and 2 has unknowns, $\alpha(t)$ and the rheological properties. Thus, information of the velocity profiles cannot directly close the system.

The Fourier transform of Eq. 1 gives

$$i\rho\omega_0\hat{u}(r,\omega) = \hat{\alpha}(\omega) + \left(\frac{\partial}{\partial r} + \frac{1}{r}\right)\hat{\tau}(r,\omega), \tag{3}$$

where $\hat{}$ denotes the Fourier-transformed function. If the unsteady flow has a dominant frequency $\omega = \omega_0$, the equation above reduces to

$$i\rho\omega_0\hat{u}(r;\omega_0) = \hat{\alpha}(\omega_0) + \left(\frac{d}{dr} + \frac{1}{r}\right)\hat{\tau}(r;\omega_0). \tag{4}$$

Here $\hat{\alpha}(\omega_0)$ is a complex amplitude of the pressure fluctuations as a complex constant. The velocity profiles are given as N-points discrete data in the radial direction, $u(r_n,t),\ n = 1,2,\cdots,N$. Substituting them into Eq. 4 forms the equation system consisting of N equations, which is much larger than the number of unknowns, i.e. the complex pressure amplitude and the rheological properties. The equation system thus can be closed. To determine the multiple unknowns, the following cost function is used:

$$F[\hat{\alpha}(\omega_0), \Pi_1, \Pi_2, \Pi_3, \cdots] = \sum_{n=0}^{N} \left| i\rho\omega_0\hat{u}(r_n;\omega_0) - \hat{\alpha}(\omega_0) - \left(\left.\frac{d}{dr}\right|_{r_n} + \frac{1}{r_n}\right)\hat{\tau}(r_n;\omega_0)\right|^2, \tag{5}$$

where $d\hat{\tau}/dr|_{r_n}$ represents the differential coefficient of $\hat{\tau}$ at $r = r_n$. The unknowns are thus

determined by minimizing the function:

$$\min F[\hat{\alpha}(\omega_0), \Pi_1, \Pi_2, \Pi_3, \cdots] \Longrightarrow \Re[\hat{\alpha}(\omega_0)], \Im[\hat{\alpha}(\omega_0)], \Pi_1, \Pi_2, \Pi_3, \cdots . \tag{6}$$

Application as in-line viscometry

Here we consider in-line 'viscometry' using the algorithm mentioned above as the first step of its applications. The equation of motion, Eq. 1 is reduced with Newton's law of viscosity, $\tau = \mu\dot{\gamma}$, into

$$\frac{\partial u}{\partial t} = \frac{1}{\rho}\alpha(t) + \frac{\mu}{\rho}\frac{1}{r}\frac{\partial}{\partial r}\left(r\frac{\partial u}{\partial r}\right). \tag{7}$$

Taking the Fourier transform of the equation and choosing a frequency component at $\omega = \omega_0$,

$$i\omega_0\hat{u}(r;\omega_0) = \frac{1}{\rho}\hat{\alpha}(\omega_0) + \nu\frac{1}{r}\frac{d}{dr}\left[r\frac{d\hat{u}(r;\omega_0)}{dr}\right], \tag{8}$$

where $\nu = \mu/\rho$ denotes kinematic viscosity. Considering the discrete data points of $u(r,t)$ at each radial position, r_n, the cost function is

$$F\left[\hat{\alpha}(\omega_0), \nu\right] = \sum_{n=1}^{N}\left|i\omega_0\hat{u}(r_n;\omega_0) - \frac{\hat{\alpha}(\omega_0)}{\rho} - \nu D_r\hat{u}(r_n;\omega_0)\right|^2, \tag{9}$$

where we defined a radial differential operator,

$$D_r = \frac{1}{r_n}\frac{d}{dr}\left(r_n\frac{d}{dr}\right)_{r_n}. \tag{10}$$

Through the optimization problem of the cost function above, the pressure difference is also determined as an unknown quantity, not given by the pressure difference measurement like in the conventional methods. Using real and imaginary parts of $\hat{u}$ and $\hat{\alpha}$, the cost function

can be simplified as

$$F\left[\hat{\alpha}(\omega_0), \nu\right] = \sum_{n=1}^{N} \left(\mathrm{Re}^2 + \mathrm{Im}^2\right), \tag{11}$$

$$\mathrm{Re} = -\omega_0 \Im[\hat{u}] - \frac{1}{\rho}\Re[\hat{\alpha}] - \nu D_r \Re[\hat{u}],$$

$$\mathrm{Im} = \omega_0 \Re[\hat{u}] - \frac{1}{\rho}\Im[\hat{\alpha}] - \nu D_r \Im[\hat{u}].$$

We used Fourier series expansion to realize the analysis explained above. The velocity and pressure gradient are represented by the Fourier series as

$$u(r_n, t) = \frac{a_0(r_n)}{2} + \sum_{k=1}^{\infty} a_k(r_n) \cos k\Delta\omega t + \sum_{k=1}^{\infty} b_k(r_n) \sin k\Delta\omega t, \tag{12}$$

$$\alpha(t) = \frac{A_0}{2} + \sum_{k=1}^{\infty} A_k \cos k\Delta\omega t + \sum_{k=1}^{\infty} B_k \sin k\Delta\omega t, \tag{13}$$

respectively, with a frequency resolution $\Delta\omega$. Here, $a_k(r_n)$ and $b_k(r_n)$ are the Fourier coefficients as a function of the radial position, and A_k and B_k are constants. Re and Im in Eq. 11 are represented using the coefficients

$$\mathrm{Re} = \omega_0 b_{\omega_0}(r_n) - \frac{1}{\rho} A_{\omega_0} - \nu D_r a_{\omega_0}(r_n), \tag{14}$$

$$\mathrm{Im} = -\omega_0 a_{\omega_0}(r_n) - \frac{1}{\rho} B_{\omega_0} - \nu D_r b_{\omega_0}(r_n), \tag{15}$$

where the subscript ω_0 denotes the Fourier coefficients corresponding to the dominant frequency, $\omega = \omega_0$. For estimation of the viscosity, there are three unknowns: ν, A_{ω_0}, and B_{ω_0}. Therefore, at least $N = 3$ is required to close the equation system. Using a larger number of N will improve the robustness of the estimation via calculation of the cost function, but may also make the estimation unstable because of measurement errors in $u(r_n, t)$.

Limitations of the present viscometry

The present viscometry has limitations on the range of viscosity to be evaluated accurately. The thickness of the viscous layer, which is defined as $\delta_{\rm v} = \sqrt{\nu/\omega}$, is an important determinant of this limitation. According to the theory of viscous fluid flow, the influence of viscosity appears only in the viscous layer for oscillating flows. To extract information of the viscosity from the velocity profiles, condition $\Delta r = r_{n+1} - r_n < \delta_{\rm v}$ (i.e. multiple data points in the viscous layer) is required. This condition means low viscosity and/or high frequency are not appropriate for our algorithm. There are also limitations in the temporal and spatial resolutions of UVP measurements; thus Δr and ω_0 should be selected as $\Delta r \sim 1$ mm and $\omega_0/(2\pi) = O(1\ \text{Hz})$. A rough approximation regarding the measurement limitations above provides $\nu \gtrsim 10\ \text{mm}^2/\text{s}$.

For highly viscous fluids, the assumption of $\delta_{\rm v} \gg R$ provides an asymptotic solution of pulsatile pipe flows as

$$u(r,t) = \frac{\Delta p}{4\mu}(R^2 - r^2)\exp(i\omega t). \tag{16}$$

The parabolic shape of the instantaneous profiles is independent of time. More over, the spatio-temporal velocity data are now not informative for determining the viscosity and pressure independently. In the cost function of Eq. 5, the first term in the right-hand side disappears, and our algorithm can determine only fraction of the pressure gradient to the viscosity.

The discussions above would be considered also in extension of the method to non-Newtonian fluids. The lower and higher limiations of the viscosity estimated above will be effectual for non-Newtonian fluids, and therefore, e.g., dilute polymer solutions having very low viscosity may not be able to be evaluated by the present rheometry. In addition to this, a range of shear rate realized in the pipe flow. We will mention the extension of the method in the concluding remarks.

Numerical validation of the viscometry

We evaluated the applicable range of our viscometry by numerical experiments using discrete velocity data generated from an exact solution of the equation of motion, Eq. 7. Assuming a trigonometrically fluctuating pressure gradient, $\alpha(t) = -\Delta P \exp(i\omega t)$, gives the exact solution expressed by Bessel functions. The applicable form of the solution for generating the discrete velocity data is then obtained via the analytical process follows (and also detailed in the Appendix):

$$u(r,t) = \frac{\Delta P}{\omega\rho}\frac{1}{\Phi_{0,R}^2 + \Psi_{0,R}^2}\left[(\Phi_{0,R}\Phi_0 + \Psi_{0,R}\Psi_0 - \Phi_{0,R}^2 - \Psi_{0,R}^2)\sin\omega t \right. \\ \left. +(\Phi_{0,R}\Psi_0 - \Psi_{0,R}\Phi_0)\cos\omega t\right], \tag{17}$$

where

$$\Phi_0(r) = \sum_{m=0}^{\infty}\phi_{0,m}, \Psi_0(r) = \sum_{m=0}^{\infty}\psi_{0,m}, \Phi_{0,R} = \Phi_0(R), \Psi_{0,R} = \Psi_0(R),$$

$$\phi_{0,m} = \frac{1}{m!m!}\left(\frac{r}{2}\sqrt{\frac{\omega}{\nu}}\right)^{2m} f_m,$$

$$f_m = \begin{cases} (-1)^{\frac{m}{2}} & m = \text{even number} \\ 0 & m = \text{odd number} \end{cases},$$

$$\psi_{0,m} = \frac{1}{m!m!}\left(\frac{r}{2}\sqrt{\frac{\omega}{\nu}}\right)^{2m} g_m,$$

$$g_m = \begin{cases} 0 & m = \text{even number} \\ (-1)^{\frac{m-1}{2}} & m = \text{odd number} \end{cases}.$$

The parameters of the geometry and the discretization were set with considering actual UVP measurements as $R = 25$ mm, $\Delta r = 1$ mm, and time resolution $\Delta t = 0.1$ s. The Frequency of the pulsation, $f_0 = \omega_0/(2\pi)$, and viscosity were examined $f_0 = 0.2, 0.5$ and 1.0 Hz, $\nu = 1.0 \times 10^{-5}$ m^2/s to 5.0×10^{-2} m^2/s with constant characteristic velocity, $U_\mathrm{m} =$

$\Delta P/(\rho\omega_0)$. In the viscosity range examined, larger viscosities reduced the velocity; however, the amplitude was sufficiently large to analyze. The Reynolds number is calculated from a root-mean-square value of the velocity fluctuations, $u_{\rm rms}$, as the characteristic velocity. It is $Re = u_{\rm rms}(2R)/\nu \approx 180$ as the maximum in the present conditions, which is sufficiently small to assume laminar flow. Examples of the calculated velocity data with $f_0 = 0.5$ Hz are shown in Fig. 1(a) and (d) for $\nu = 1.0 \times 10^{-5}$ m^2/s and 1.0×10^{-4} m^2/s, respectively.

The velocity maps are displayed in half of the pipe, $r = 0$ to R, and for two periods of pulsation. The velocity is represented by periodic changes in color contour due to pressure fluctuation. There is a phase delay near the pipe wall as the result of viscous shear stress. The degree of the delay depends on the viscosity; that is, the viscous effect seems to penetrate deeper into the interior of the pipe flow in Fig. 1(d). Instantaneous velocity profiles corresponding to the velocity maps at different phases of the oscillations display the differences in the viscous effect more clearly [Fig. 1(b) and (e)]. In the less-viscous case [Fig. 1(b)], the viscous effects are limited to the region near the pipe wall, $r \gtrsim 17$ mm, and the instantaneous velocity profiles are much flatter in the inner regions, $r \lesssim 17$ mm. In this inner region, the velocity fluctuation is determined only by the periodic pressure fluctuations and the velocity profiles have no information about viscosity because $D_r a_{\omega_0}$ and $D_r b_{\omega_0}$ in Eqs. 14 and 15 disappear. The instantaneous radial position taking the maximum velocity distributes from $r = 20 - 23$ mm, and the largest radial position, $r \approx 23$ mm, has good correspondence with the estimated thickness of the viscous layer, $\delta_{\rm v} \approx 1.8$ mm ($R - \delta_{\rm v} \approx 23.2$ mm). This value of $\delta_{\rm v}$ is comparable to the spatial resolution, $\Delta r = 1$ mm set in our numerical experiment and may complicate the estimation of viscosity because of insufficient resolution for the viscous layer. In contrast with the lower viscosity case, the velocity profiles for $\nu = 1.0 \times 10^{-4}$ m^2/s shown in Fig. 1(e) represent viscous effect reaching the center of the pipe. The instantaneous radial position taking the maximum velocity distributes over a wider region and the largest position may correspond to the estimated thickness of viscous layer, $\delta_{\rm v} \approx 5.6$ mm. In this case, the whole region of r provides information related to the viscosity and the estimation

can be carried out with high accuracy.

To estimate ν with our algorithm, we extracted the Fourier components corresponding to $f = f_0$, and approximated the radial distributions of their real and imaginary parts, $a_{\omega_0}(r)$ and $b_{\omega_0}(r)$, by fitting with an 8th-order power series. This reduced the numerical error due to the discretization in the process of taking the derivative. Figure 1(c) and (f) show the profiles for each condition of ν, where the individual symbols represent discrete data points in the radial direction. The profiles of a_{ω_0} and b_{ω_0} represent the characteristics observed in the instantaneous velocity profiles mentioned above. Here, the order of the polynomial (eight) was empirically determined.

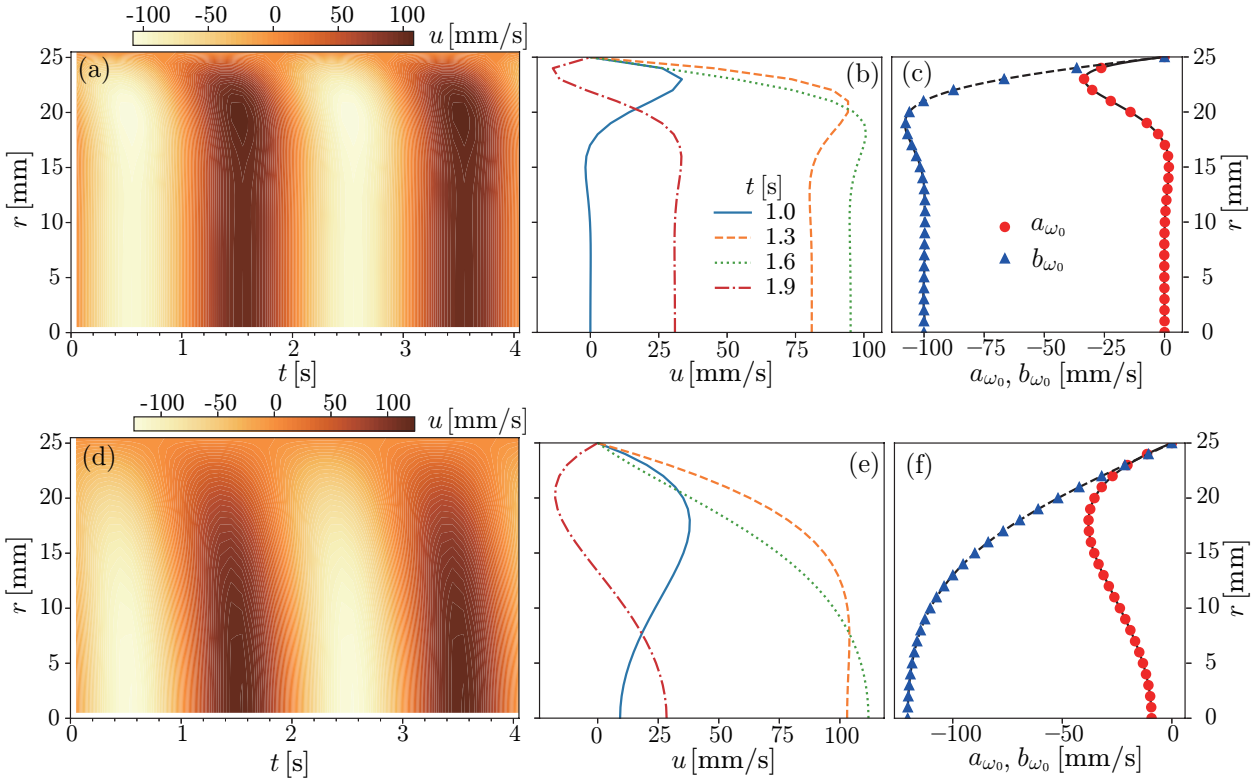

Figure 1: Examples of the analysis; panels in the first (a,b,c) and the second rows (d,e,f) are for $\nu = 1.0 \times 10^{-5}$ m^2/s and 1.0×10^{-4} m^2/s. (a)(d) Spatio-temporal velocity distributions in two periods of pulsatile pipe flow with $f_0 = 0.5$ Hz. (b)(e) Instantaneous radial velocity profiles, and profiles of the real and imaginary components of the Fourier-transformed velocity corresponding to $f = f_0$.

The viscosity was estimated using $a_{\omega_0}(r)$ and $b_{\omega_0}(r)$ in the cost function, Eq. 11, for the frequency and viscosity mentioned above. In the optimization process of the cost function,

the range and resolution of the viscosity were fixed at ±20% and 0.1% of the set values. The estimated viscosities are summarized in Fig. 2 as the variation of ν normalized by the set viscosity, ν_{set}, with respect to the normalized thickness of the viscous layer, δ_{v}/R. The viscosity was correctly estimated in the range of $0.2 < \delta_{\mathrm{v}}/R \leq 1.1$ but had large deviations outside this range. The lower limit of the applicable range, $\delta_{\mathrm{v}}/R = 0.2$, corresponds to $5\Delta r$. This suggests that multiple data points are required to resolve the viscous layer to estimate the viscosity correctly. For practical use, the maximum estimation error of within 3%, of our numerical experiment is accepted. However, for use in industrial pipes, the velocity data would contain larger measurement errors. This uncertainty may be augmented in the process of viscosity estimation in addition to the theoretical limitations of the method. Thus, the applicable range would not be much wider in the practical situations than in the present study despite allowing for considerable estimation errors.

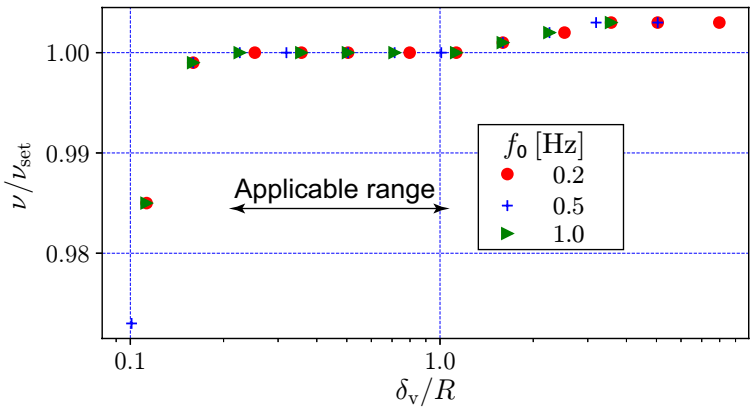

Figure 2: Estimated viscosity normalized by the set viscosity, ν/ν_{set}, as a function of the thickness of the viscous layer, δ_{v}/R. Three different oscillation frequencies were examined.

Experimental evaluation of applicability

Experimental setup and procedure

We experimentally evaluated the applicability of our in-line viscometry. The experimental setup is a laboratory pipe loop consisting of a jacket tank for storage, 2-inch standard stainless

pipes with a length of 3 m, a rotary lobe pump, and a test section for measuring the velocity profile (Fig. 3). The test section comprised an acrylic resin with a diameter of $2R = 46$ mm to improve ultrasonic transmission into the test fluid, 300 cSt silicone oil ($\rho = 970$ kg/m^3, $\mu = 0.29$ Pa·s, Shin-Etsu Chemical Co., Ltd.) as a representative Newtonian fluid. The tilting angle of the 4 MHz ultrasonic transducer to the normal line of the pipe wall, θ_1, was designed for efficient ultrasound transmission and considering the angle of the measurement line in the test fluid, θ_2. From the speed of sound in the acrylic resin and the test fluid, $c_1 = 2730$ m/s and $c_2 = 980$ m/s, the angles were determined as $\theta_1 = 35°$ and $\theta_2 = 12°$, respectively. Ultrasonic echo signals scattered by seeding particles dispersed in the test fluid (CHP20P, apparent density: 1010 kg/m^3, diameter: 75–150 μm, Mitsubishi Chemical Co. Ltd., Japan) were recorded and processed by a UVP monitor model Duo (Met-Flow S.A.). The instantaneous profiles of the velocity component in the measurement line, $u_\xi(\xi, t)$, were then converted into radial profiles of the pipe-axial velocity component, $u(r, t)$, by assuming one-directional flow as $u = u_\xi / \sin\theta_2$.

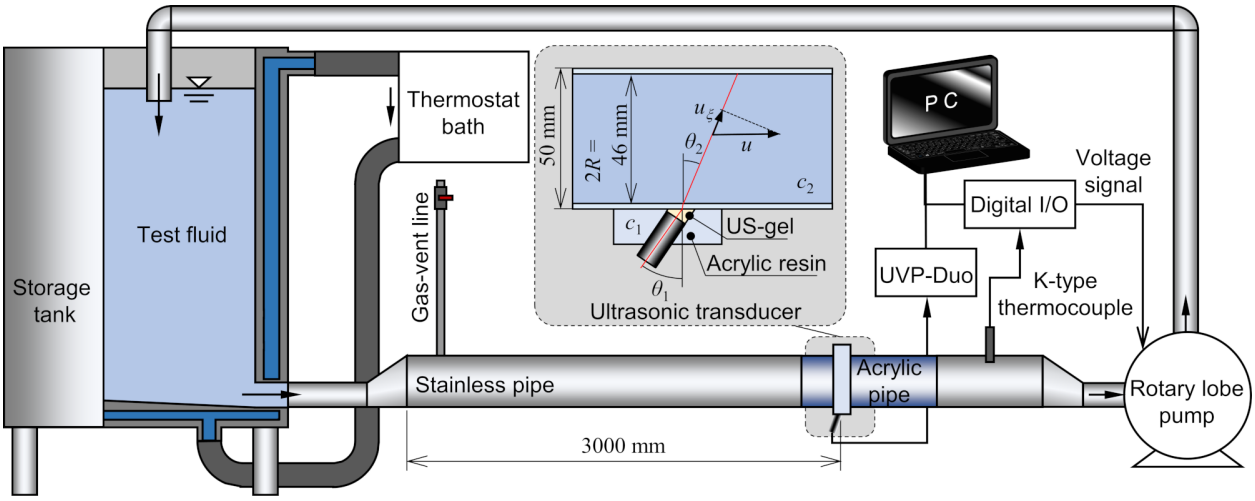

Figure 3: Schematic diagram of the experimental setup for evaluating the proposed in-line viscometry. This consisted of a stainless-steel jacket tank, stainless-steel pipes, a rotary lobe pump, and a test section made of acrylic resin to hold an ultrasonic transducer for velocity profile measurements.

To simulate the transient changes in viscosity, we modified the temperature of the test fluid by increments and decrements of the set temperature used in the laboratory tests.

Because of high heat-exchange rate of the pipe system due to the stainless-steel pipes, the temperature of the test fluid was adjusted to room temperature in an hour. The corresponding temperature variation in the test fluid was recorded via a thermocouple set near the test section.

The flow rate was intentionally oscillated using the inverter control of the pump as a trigonometric function with $f_0 = 1$ Hz, and a maximum and minimum flow rate of 0.29 and 0.06 m^3/h, respectively. The corresponding thickness of the viscous layer was approximately 5 mm, which is the same order of magnitude as the radius of the pipe (23 mm). Measurement of the velocity profile was performed for 10,000 s with a 50-ms sampling period. The axial velocity was obtained at each time and radial position, r, with spatial resolution $\Delta r = 0.47$ mm. The measurement volume had a disk-like shape whose diameter and length correspond to those of the ultrasonic wave packet, ~ 5 mm and ~ 1 mm, respectively.

Results

An example of the spatio-temporal velocity distribution measured by UVP is shown in Fig. 4(a), where the color represents the instantaneous local velocity. The top and bottom boundaries of the figure correspond to the opposite pipe walls, and the transducer was set at the negative side of r. The distribution represents the set pulsation flow for 3 s, which corresponds to three periods of the pulsation. The instantaneous velocity profiles appear symmetric in the radial direction excluding the far-side wall of the transducer, $r/R \sim 1$. This asymmetric error near the wall was due to multiple reflections of the ultrasonic waves. The real and imaginary Fourier components corresponding to the set frequency of the oscillation f_0 extracted from the velocity distribution are shown in Fig. 4(b). Even with this strong filtering process, the profiles have deviations and are not sufficiently smooth to calculate numerical differentiations. These deviations were due to common problems in velocity profile measurements, such as an accidental blank of tracer particles and the finite velocity resolution; these are unavoidable in real situations.

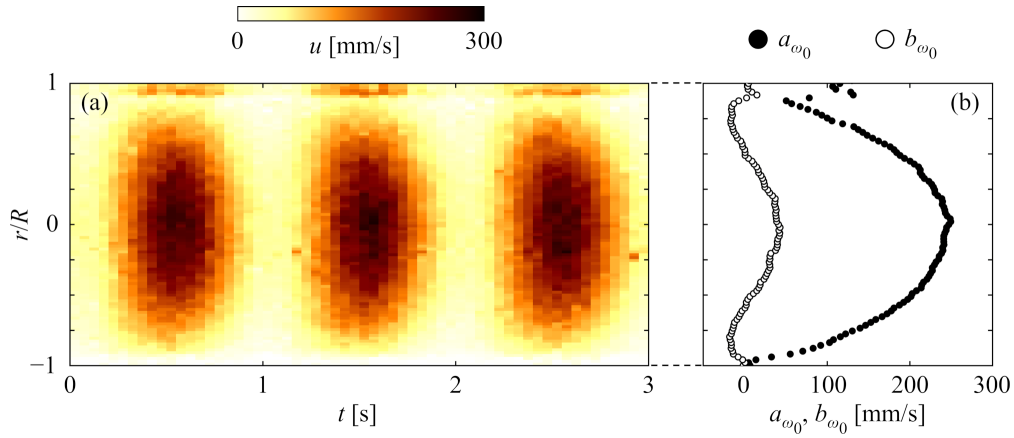

Figure 4: (a) Spatio-temporal velocity map measured by ultrasonic velocity profiling. (b) Profiles of the real and imaginary parts of the velocity fluctuations, $\Re[\hat{u}]$ and $\Im[\hat{u}]$, which correspond to the main pulsation frequency of the velocity fluctuation, f_0.

Here, we describe the estimation of the viscosity from the velocity data. The actual velocity data measured by UVP had considerable deviations and the radial profiles are not so smooth even after strong filtering by extracting the single Fourier component, as shown in Fig. 4(b). This deviations would be augmented in the process calculating numerical differentiations in Eqs. 14 and 15 to calculate the cost function, Eq. 11. Therefore, we performed local cubic-curve fitting with the neighboring 12 data points on $\Re[\hat{u}(r)]$ and $\Im[\hat{u}(r)]$ at each radial point, r_n, with Gaussian weighting. This treatment reduced error for each profiles. The cost function was then calculated for the parameter space $(|\alpha|, \mu)$, where $|\alpha|$ corresponds to the amplitude of the pressure fluctuations at $f = f_0$. Phase information for $\alpha(f = f_0)$, which was originally required for the calculation was removed by the initial adjustment of the phase of velocity fluctuation for taking the Fourier transformation. Exploring the parameter space with fine resolution is time consuming. Therefore, we used a random search method to determine the parameter point with the minimum cost function. Figure 5 shows the distribution of the cost function explored in the parameter space, where each dot and its color represent the parameter sets to be estimated and the corresponding value of the cost function. Randomly distributed dots are concentrated toward the point indicated by the star symbol at which the cost function takes a minimum value under the set resolution.

The corresponding parameter set represents the appropriate viscosity μ estimated from the velocity data.

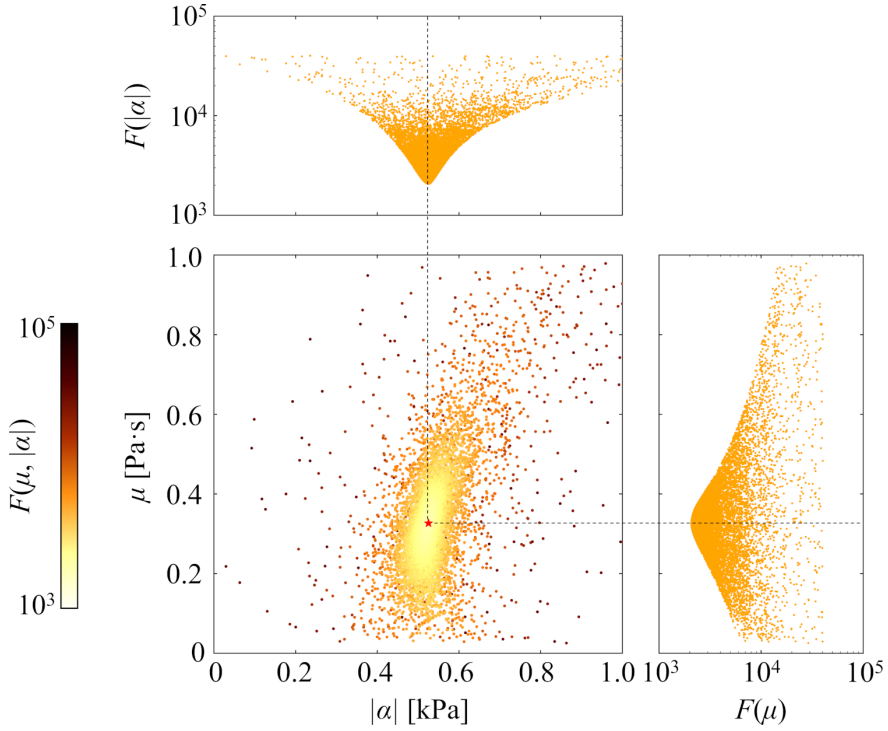

Figure 5: Distribution of the cost function to determine the appropriate viscosity, μ, and pressure amplitude, $|\alpha|$, from the velocity data, where each dot and its color represent points in the parameter space, $(|\alpha|, \mu)$, and a corresponding value of the cost function, F. The star symbol indicates the point at which F takes a minimum value.

The procedure described above was performed on each 10-s-long section with time steps of $\Delta t = 50$ ms of the velocity data measured by UVP during gradual temperature variation. The effective time resolution of the evaluation was therefore 10 s. The temperature of the test fluid measured by the thermocouple, T, increased from approximately 15 to 30°C in 5000 s, and then decreased to the 15°C in the subsequent 5000 s [Fig. 6(a)]. Here, the color code represents the probability density function (PDF) of the temperature fluctuations in each 10 s period. Figure 6(b) shows the corresponding time variation of the viscosity determined using our in-line viscometry. The color code also represents the PDF of the estimated μ; the central, highly probable values are indicated by darker colors. The viscosity varies in an opposite manner to the temperature because of the negative dependence of μ on T. The

broken lines in Fig. 6(a) and Fig. 6(b) indicate $T = 25°C$ and the reference value of the viscosity at that temperature, $\mu = 0.29$ Pa·s, respectively. The viscosity varies around the reference value during the temperature variation. Summarizing the results above, our in-line viscometry can uniquely and accurately determine the viscosity even when it undergoes transient variations, and capture its time variation with a sufficiently high time resolution of 10 s.

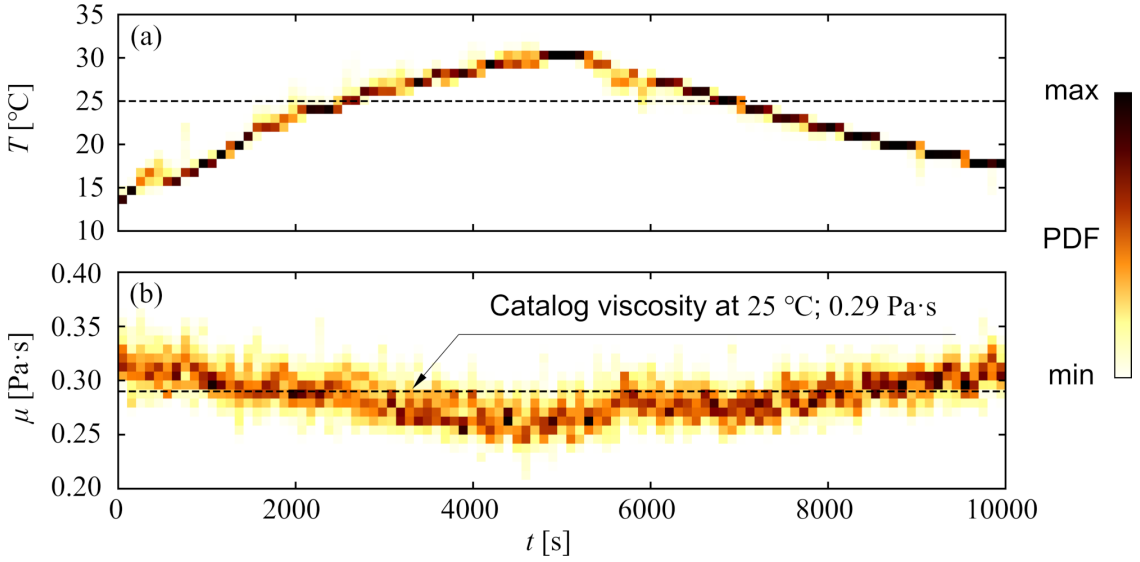

Figure 6: Time variation of (a) temperature, T, and (b) the corresponding viscosity, μ, estimated by in-line viscometry. The dashed lines in the panels indicate $T = 25°C$ and the reference value of $\mu = 0.29$ Pa·s at temperature $T = 25°C$, respectively

Concluding remarks

We proposed and demonstrated the concept of non-intrusive in-line rheometry. This method is capable of capturing transient rheological properties based on the measurement of the ultrasonic velocity profile in pipe flows. Importantly, it does not require the insertion of probes, in contrast with conventional methods. Our in-line rheometry uses time variations of the velocity profiles and analyzes them using the equation of motion that describes one-directional unsteady flows in a pipe. The analysis in the frequency domain allows us to deal with pressure fluctuations, which otherwise have to be measured in conventional methods.

the applicable range of our method was determined based on thickness of the viscous layer on the pipe wall, $\delta_{\mathrm{v}} = \sqrt{\nu/(2\pi f_0)}$. The viscosity information is limited in the viscous layer, and thus the velocity-profile measurement is required to resolve the layer. A much thicker viscous layer than the pipe radius results in a loss viscous information. We evaluated the applicable range of our method with numerical experiments using solutions of the pulsatile flows with different frequency of pressure fluctuations, f_0, and viscosity, ν. In actual industrial situations, the range should be 10 mm^2/s $\lesssim \nu \lesssim O(10^3)$ mm^2/s. Finally, in-line viscometry was performed on a laboratory pipe flow facility consisting of 2-inch pipes and a rotary pump with 300 cSt silicone oil as the test fluid. The instantaneous viscosity of the test fluid was uniquely and accurately determined, and its variation due to the temperature variation was captured with 10-s effective time resolution.

Seeking the primary frequency component of unsteady pipe flows f_0 has importance for actual applications of the present in-line rheometry in industry. Unlike USR, in which the frequency is given as the set oscillation frequency of cylinder, the in-line rheometry expects to utilize a characteristic frequency of intrinsic pulsations in pipe flows, which is usually given by length, diameter, configurations of pipelines, and pump characteristics in individual facilities. Its applicability in industrial situations will be evaluated in the next step of the study. Otherwise in test facilities with high controllability of the flow rate of a pump, the present method would be surely applied.

We had initially designed our method as in-line 'rheometry'; it can also be extended to obtain shear-rate-dependent viscosity. In this case, the effective viscosity is determined locally at each radial position, which has a different shear rate. The viscosity curve provides the range of shear rates realized in the pipe flow, and thus the shear-rate-dependent viscosity will be evaluated in the range. In contrast with conventional methods, the use of appropriate rheology models (e.g. the Maxwell model) may make it possible to evaluate the viscoelasticity of test fluids. For target fluids with unknown rheological properties, as an idea, the appropriate model will be chosen to minimize the cost function. These extensions

of our method also will be the next steps of the study.

Acknowledgement

This research was supported by Adaptable and Seamless Technology transfer Program through Target-driven R&D (A-STEP) from the Japan Science and Technology Agency(JST).

Appendix

Substituting $\alpha(t) = -\Delta P \exp(i\omega t)$ into Eq. 7, the equation of motion of the pulsatile pipe flow is derived as

$$\frac{\partial^2 u}{\partial r^2} + \frac{1}{r}\frac{\partial u}{\partial r} - \frac{1}{\nu}\frac{\partial u}{\partial t} = \frac{\Delta P}{\nu\rho}\exp(i\omega t). \tag{18}$$

Assuming the velocity, u, is

$$u(r,t) = U(r)\exp(i\omega t), \tag{19}$$

Eq. (18) can be rewritten as

$$\frac{d^2 U}{dr^2} + \frac{1}{r}\frac{dU}{dr} - \frac{i\omega}{\nu}U = \frac{\Delta P}{\nu\rho}. \tag{20}$$

This is in a Bessel equation, which has a well-known solution. We define a complex variable, ζ, that modifies the radial coordinate r,

$$\zeta = (i-1)\, r\sqrt{\frac{\omega}{2\nu}}. \tag{21}$$

Satisfying the no-slip condition at the pipe wall and with finite velocity along with the axis of the flow in the pipe, the spatio-temporal velocity distribution is obtained as

$$u(r,t) = \frac{i\Delta P}{\omega\rho}\left[1 - \frac{J_0(\zeta)}{J_0(\zeta)_{r=R}}\right]\exp(i\omega t). \tag{22}$$

To calculate the discretized numerical data, $J_{0,r=R}$ and J_0 were decomposed into the real and imaginary parts and expressed as an infinite series as

$$J_0 = \Phi_0(r) + i\Psi_0(r) = \sum_{m=0}^{\infty} \phi_{0,m}(r) + i \sum_{m=0}^{\infty} \psi_{0,m}(r), \tag{23}$$

$$J_{0,r=R} = \Phi_{0,R} + i\Psi_{0,R} = \sum_{m=0}^{\infty} \phi_{0,Rm} + i \sum_{m=0}^{\infty} \psi_{0,Rm}. \tag{24}$$

From these, Eq. (22) is modified to

$$u(r,t) = \frac{i\Delta P}{\omega\rho}\left[1 - \frac{\Phi_0 + i\Psi_0}{\Phi_{0,R} + i\Psi_{0,R}}\right](\cos\omega t + i\sin\omega t). \tag{25}$$

Finally, taking the real part of the equation above gives Eq. 17 to provide discretized data for the numerical experiment.

We note that $u(r = 0, t) \neq \Delta P/(\omega\rho) = U_{\mathrm{m}}$, because $\phi_{0,m=0}(r = 0) = 1$ and thus $\Phi_0(r = 0) = 1$, while $\Psi_0(r = 0) = 0$. The velocity fluctuation at the center of pipe becomes

$$\begin{aligned} u(0,t) &= \frac{\Delta P}{\omega\rho}\frac{1}{\Phi_{0,R}^2 + \Psi_{0,R}^2}\left[(\Phi_{0,R} - \Phi_{0,R}^2 - \Psi_{0,R}^2)\sin\omega t - \Phi_{0,R}\cos\omega t\right] \\ &= -\frac{\Delta P}{\omega\rho}\sin\omega t + \frac{\Delta P}{\omega\rho}\frac{1}{\Phi_{0,R}^2 + \Psi_{0,R}^2}\left(\Phi_{0,R}\sin\omega t - \Phi_{0,R}\cos\omega t\right). \end{aligned} \tag{26}$$

The second term in the equation above is the viscous contribution to the velocity.

References

(1) Wunderlich, T.; Brunn, P. Ultrasound pulse Doppler method as a viscometer for process monitoring. *Flow Meas. Instrum.* **1999**, *10*, 201–205.

(2) Takeda, Y., Ed. *Ultrasonic Doppler velocity profiler for fluid flow*; Springer Science & Business Media: Tokyo, 2012; Vol. 101.

(3) Ouriev, B.; Windhab, E. J. Rheological study of concentrated suspensions in pressure-driven shear flow using novel in-line ultrasound Doppler method. *Exp. Fluids* **2002**, *32*, 204–211.

(4) Ouriev, B.; Windhab, E.; Braun, P.; Zeng, Y.; Birkhofer, B. Industrial application of ultrasound based in-line rheometry: Visualization of steady shear pipe flow of chocolate suspension in pre-crystallization process. *Rev. sci. Instrum.* **2003**, *74*, 5255–5259.

(5) Wiklund, J.; Standing, M. Application of in-line ultrasound Doppler-based UVP-PD rheometry method to concentrated model and industrial suspensions. *Flow Meas. Instrum.* **2008**, *19*, 171–179.

(6) Choi, Y.; Milczarek, R.; Fleck, C.; Garvey, T.; McCarthy, K.; McCarthy, M. In-line monitoring of tomato concentrate physical properties during evaporation. *J. Food Process Eng.* **2006**, *29*, 615–632.

(7) Ouriev, B.; Windhab, E. Transient flow of highly concentrated suspensions investigated using the ultrasound velocity profiler–pressure difference method. *Meas Sci. Ttechnol.* **2003**, *14*, 1963.

(8) Birkhofer, B. H.; Jeelani, S. A.; Windhab, E. J.; Ouriev, B.; Lisner, K.-J.; Braun, P.; Zeng, Y. Monitoring of fat crystallization process using UVP–PD technique. *Flow Meas. Instrum.* **2008**, *19*, 163–169.

(9) Fischer, P.; Ouriev, B.; Windhab, E. J. Macroscopic Pipe Flow of Micellar Solutions Investigated by Ultrasound Doppler Velocimetry. *Tenside Surfact. Det.* **2009**, *46*, 140–144.

(10) Wiklund, J.; Rahman, M.; Håkansson, U. In-line rheometry of micro cement based grouts–A promising new industrial application of the ultrasound based UVP+ PD method. *Appl. Rheol.* **2012**, *22*.

(11) Rahman, M.; Wiklund, J.; Kotzé, R.; Håkansson, U. Yield stress of cement grouts. *Tunn. Undergr. Sp. Tech.* **2017**, *61*, 50–60.

(12) Wiklund, J.; Shahram, I.; Stading, M. Methodology for in-line rheology by ultrasound Doppler velocity profiling and pressure difference techniques. *Chem. Eng. Sci.* **2007**, *62*, 4277–4293.

(13) Kotze, R.; Wiklund, J.; Haldenwang, R. Optimisation of Pulsed Ultrasonic Velocimetry system and transducer technology for industrial applications. *Ultrasonics* **2013**, *53*, 459–469.

(14) Pfund, D. M.; Greenwood, M. S.; Bamberger, J. A.; Pappas, R. A. Inline ultrasonic rheometry by pulsed Doppler. *Ultrasonics* **2006**, *44*, e477–e482.

(15) Derakhshandeh, B.; Viassopoulos, D.; Hatzikiriakos, S. G. Thixotropy, yielding and ultrasonic Doppler velocimetry in pulp fiber suspensions. *Rheol. Acta* **2012**, *51*, 201–214.

(16) Manneville, S.; Bécu, L.; Colin, A. High-frequency ultrasonic speckle velocimetry in sheared complex fluids. *Eur. Phys. J. Appl. Phys.* **2004**, *28*, 361–373.

(17) Gallot, T.; Perge, C.; Grenard, V.; Fardin, M. A.; Taberlet, N.; Manneville, S. Ultrafast ultrasonic imaging coupled to rheometry: Principle and illustration. *Rev. Sci. Instrum.* **2013**, *84*, 045107.

(18) Tasaka, Y.; Kimura, T.; Murai, Y. Estimating the effective viscosity of bubble suspensions in oscillatory shear flows by means of ultrasonic spinning rheometry. *Exp. Fluids* **2015**, *56*, 1–13.

(19) Yoshida, T.; Tasaka, Y.; Murai, Y. Rheological evaluation of complex fluids using ultrasonic spinning rheometry in an open container. *J. Rheol.* **2017**, *61*, 537–549.

(20) Tasaka, Y.; Yoshida, T.; Rapberger, R.; Murai, Y. Linear viscoelastic analysis using frequency-domain algorithm on oscillating circular shear flows for bubble suspensions. *Rheol. Acta* **2018**, *57*, 229–240.

(21) Yoshida, T.; Tasaka, Y.; Murai, Y. Efficacy assessments in ultrasonic spinning rheometry: Linear viscoelastic analysis on non-Newtonian fluids. *J. Rheol.* **2019**, *63*, 503–517.

(22) Yoshida, T.; Tasaka, Y.; Murai, Y. Effective viscoelasticity of non-Newtonian fluids modulated by large-spherical particles aligned under unsteady shear. *Phys. Fluids* **2019**, *31*, 103304.

(23) Yoshida, T.; Tasaka, Y.; Tanaka, S.; Park, H.; Murai, Y. Rheological properties of montmorillonite dispersions in dilute NaCl concentration investigated by ultrasonic spinning rheometry. *Appl. Clay Sci.* **2018**, *161*, 513–523.

(24) Yoshida, T.; Tasaka, Y.; Fischer, P. Ultrasonic spinning rheometry test on the rheology of gelled food for making better tasting desserts. *Phys. Fluids* **2019**, *31*, 113101.

Graphical TOC Entry